Proceedings of the 9th U.S. National and 10th Canadian Conference on Earthquake Engineering
Compte Rendu de la 9ième Conférence Nationale Américaine et
10ième Conférence Canadienne de Génie Parasismique
July 25-29, 2010, Toronto, Ontario, Canada • Paper No 584

RELIABILITY-BASED EVALUATION OF DESIGN PROCEDURE FOR STEEL SELF-CENTERING MOMENT FRAMES

Gordana Herning[1], Maria E. M. Garlock[2] and Erik Vanmarcke[3]

ABSTRACT

Self-centering moment-resisting frames (SC-MRFs) have the potential to eliminate structural damage under a design basis earthquake and return to their original vertical position following a major earthquake. The objective of this study is to validate an existing design procedure for SC-MRFs. This study examines the response of a 3, 9, and 20 story SC-MRF subject to one thousand artificially generated design (DBE) and maximum considered (MCE) ground motions. The predicted maximum roof drift, story drift, and connection rotation are compared, in probabilistic terms, to the demand obtained in the nonlinear analyses. This data is used to recommend means to improve the existing design procedure and to generate fragility curves for the structure. The results will be used to develop a reliability-based seismic design procedure for these SC-MRF connection details.

Introduction

Motivation for recent development of performance-based design recommendations for steel self-centering frames (Garlock et al. 2007) comes from the results obtained over the last decade in experimental and analytical investigations of these systems in seismic applications (Ricles et al. 2001, Christopolous et al. 2002, Garlock et al. 2005, and Chou et al. 2006). Research shows that these highly ductile systems resist structural damage after repeated inelastic response cycles under the design level earthquakes. Due to post-tensioning that enables self-centering, residual drift after an earthquake is eliminated. Supplemental connection elements such as top-and-seat angles (Garlock et al. 1998), steel bars (Christopolous et al. 2002), friction devices (Rojas et al. 2005) or plates (Chou et al. 2006) are provided to increase energy dissipation (ED) and to detract structural damage from the main frame elements. Connection behavior, characteristic for PT frames under cyclic loading, includes opening and closing of a horizontal gap at the beam-column interface. This is quantified by the relative rotation between the beam tension flange and the column flange, θ_r, as shown in Fig. 1.

Prior studies related to the existing design procedure for the SC-MRFs were based on a six story prototype building subjected to six ground motions (Garlock et al. 2007), which was the extent of computational capabilities at the time. Recent technological advances enable the number of computational simulations that was previously not feasible. High performance computing facilities now allow running thousands of nonlinear analyses of these prototype models in a day. In the current study, we subjected 3, 9 and 20 story prototypes to over a

[1]Graduate Student, Dept. of Civil and Environmental Engineering, Princeton University, Princeton, NJ 08544
[2]Assistant Professor, Dept. of Civil and Environmental Engineering, Princeton University, Princeton, NJ 08544
[3]Professor, Dept. of Civil and Environmental Engineering, Princeton University, Princeton, NJ 08544

thousand seismic events, including natural seismic records (Herning et al. 2009) and synthetically generated ground motions. Structural response to both types of events confirms the validity of using artificial ground motions, which can be a convenient substitute in the absence of a sufficient number of representative natural records for a particular area.

The dataset obtained from the analyses using artificial ground motions was the basis for a reliability study of the SC-MRFs, in which we assessed the probability of the system demand exceeding its capacity. Using a closed-form relationship for θ_r at which post-tensioning strands yield (Garlock et al. 2007), we express the system reliability in terms of the likelihood of reaching the limit state of strand yielding. We also evaluated the effectiveness of the response predictions that were made in the design process. The predicted seismic demands, such as connection relative rotation (θ_r in Fig. 1), roof drift, and story drift, were compared to those obtained in the nonlinear analyses, to study the effects of the design parameters, and to recommend the means of improving the design procedure.

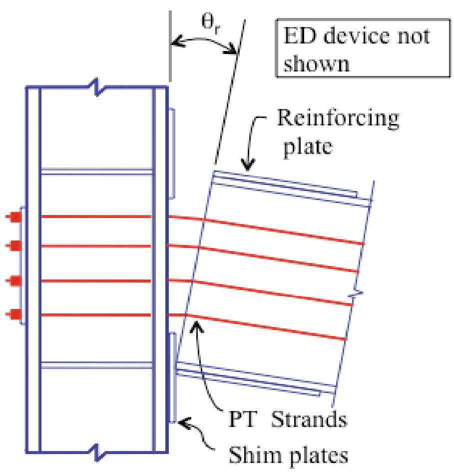

Figure 1. Deformation at decompression in a PT connection.

Prototype Design

Three, nine and twenty story prototype buildings were designed for a high-risk seismic zone and stiff soil conditions, using the performance based design procedure described in Garlock et al. (2007) and the provisions of ASCE Design Standard 7-05. All members are assumed to have a nominal yield stress of 50 ksi and gravity loads consistent with an office building in Los Angeles, CA. Floor plans, elevations, member sizes, and connection details of the three prototypes are shown in Fig. 2. SC-MRFs occupy only the interior bays at the perimeter of the buildings, to reduce the potential of bi-axial bending at the corner columns and out-of plane bending of the SC-MRFs. Composite action between the gravity framing and the slab is assumed in the areas that are shaded in plan. Floor beams perpendicular to the MRFs are collector beams, which transfer the inertia forces from the slab to the frames. Collector beam designs are prototype-specific and are given in Garlock et al. (2009). The 3 and 9 story prototypes each have eight collector beams framing into a MRF at every level above grade, while the 20 story building has seven. The collector beam stiffness and strength for the 3 and 9 story are 65 kips/inch and 98 kips, respectively. The 20 story prototype has collector beam stiffness and strength of 86 kips/inch and 108 kips, respectively. The fundamental periods for the 3, 9, and 20 story prototypes are 1.1, 3.3, and 3.4 seconds, respectively.

The existing design procedure for SC-MRFs classifies the designs as special moment frames in the ASCE 7-05. The 3 story prototype was designed following the Equivalent Lateral Force (ELF) procedure. Because the fundamental periods for the 9 and 20 story prototypes are larger than the maximum permitted by the code for using the ELF procedure, the Modal

Response Spectrum Analysis (RSA) was used for the design of the two taller prototypes. The distinction between the two procedures is significant because of the difference in their recommended limits for the interstory drift, and the absence of a lower bound for the spectral acceleration in the design response spectrum when using the RSA procedure. Therefore, the RSA standard implicitly permits the design of more flexible steel MRFs than does the ELF procedure.

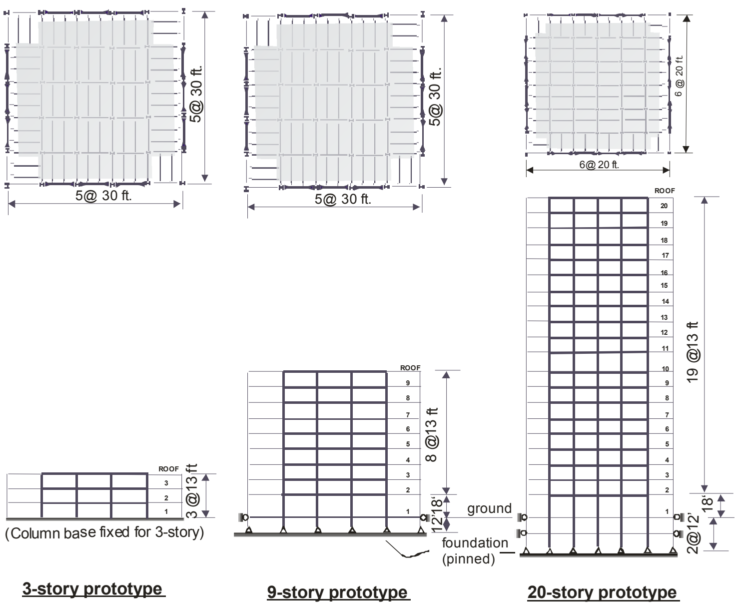

		Beam	Interior column	t_{cp} (in)	L_{cp} (in)	N_s	T_o (k)
3-st	RF	W24X146	W14X233	1	36	12	368
	3	W24X146	W14X233	1	36	16	344
	2	W24X162	W14X257	1	36	12	355
9-story	RF	W18X106	W14X159	0.75	66	16	344
	9	W18X106	W14X159	0.75	66	16	327
	8	W18X106	W14X159	0.75	66	16	378
	7	W21X111	W14X233	0.75	66	16	430
	6	W21X122	W14X233	0.75	66	16	490
	5	W24X131	W14X233	0.75	66	16	516
	4	W27X146	W14X311	0.75	66	20	538
	3	W27X161	W14X311	1	66	20	613
	2	W30X211	W14X426	1	66	24	735
20-story	RF	W18X97	W14X211	0.75	36	16	343
	20	W18X97	W14X211	0.75	36	16	343
	19	W18X97	W14X211	0.75	36	16	343
	18	W18X97	W14X211	0.75	36	16	343
	17	W18X97	W14X211	0.75	36	16	376
	16	W18X97	W14X211	0.75	36	16	426
	15	W30X148	W14X342	1	36	16	527
	14	W30X148	W14X342	1	36	16	518
	13	W30X148	W14X342	1	36	20	470
	12	W30X148	W14X342	1	36	20	428
	11	W30X148	W14X426	1	36	20	470
	10	W30X173	W14X426	1	36	24	614
	9	W30X173	W14X426	1	36	24	627
	8	W30X173	W14X426	1	36	24	639
	7	W30X173	W14X426	1	36	24	652
	6	W30X173	W14X500	1	36	24	690
	5	W30X173	W14X500	1	36	24	702
	4	W30X173	W14X605	1	36	24	715
	3	W36X230	W14X605	1.25	36	28	717
	2	W36X230	W14X605	1.25	36	28	878

Figure 2. Prototype geometry, sizes and connection details.

The existing design procedure for SC-MRFs classifies the designs as special moment frames in the ASCE 7-05. The 3 story prototype was designed following the Equivalent Lateral Force (ELF) procedure. Because the fundamental periods for the 9 and 20 story prototypes are larger than the maximum permitted by the code for using the ELF procedure, the Modal Response Spectrum Analysis (RSA) was used for the design of the two taller prototypes. The distinction between the two procedures is significant because of the difference in their recommended limits for the interstory drift, and the absence of a lower bound for the spectral acceleration in the design response spectrum when using the RSA procedure. Therefore, the RSA standard implicitly permits the design of more flexible steel MRFs than does the ELF procedure.

The interior column sizes were controlled by the strong column–weak beam criterion. The exterior column size was uniformly set at two sizes smaller than the interior column size. The beam size was governed by either (1) beam compactness criteria, or (2) beam local buckling criteria based on combined moment and axial load stresses, or (3) decompression moment criterion required for self-centering. The last criterion requires that $M_d \geq 0.6\ M_a$, where M_d is the minimum decompression moment (point 1 in Fig. 1a), and M_a is the moment at which the energy dissipating devices change stiffness (point 2 in Fig. 1a). The beam sections in most lower stories of the 9 and 20 story prototype were controlled by the criterion that prevents connection decompression under wind forces, i.e. $M_d > M_{wind}$.

Ground Motions

In this study we used a subset of the ground motions available in the Pacific Earthquake Engineering Research (PEER) Center NGA (Next Generation Attenuation) strong motion database (Chiou et al. 2008). A selection of 3243 records from 117 earthquakes was used to develop an attenuation model for generating region-specific artificial ground motions, as described in Pant and Vanmarcke (2009). Two empirical attenuation models were developed to estimate: (1) strong motion intensity measures, such as Arias Intensity and strong motion duration, and (2) frequency measures, i.e., central frequency and bandwidth factor. These indicators characterize a ground motion with its amplitude, frequency content, and strong motion duration. The concept for the present attenuation relationship was derived from the model proposed by Sabetta and Pugliese (1996), and represents an improvement with respect to the previously attained energy content at lower frequencies and the event variability.

Ground motion indicators, which contribute to a seismic hazard level at a chosen site, are the magnitude, M, epicentral distance, R, and ε, the measure of uncertainty or deviation of a ground motion from a predicted level. Two levels of seismic hazard are defined in the NEHRP (Building Seismic Safety Council 1997) provisions: the design basis earthquake (DBE), with 50% probability of exceedance in 50 years, and the maximum considered earthquake (MCE), with 2% probability of exceedance in 50 years. The DBE is used in current seismic design provisions, such as IBC 2000 (International 2000) to establish design earthquake forces, and is taken as 2/3 of the intensity of the MCE.

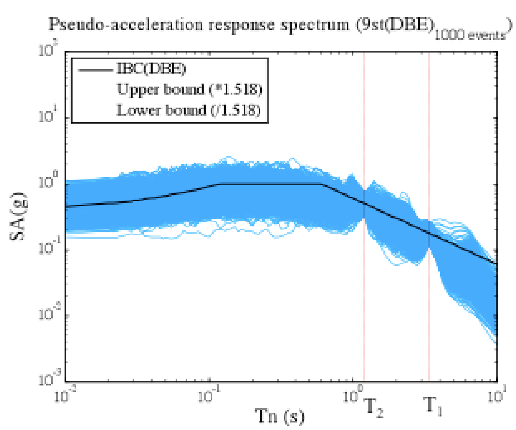

Figure 3. Pseudo-acceleration response spectrum of selected artificial ground motions for 9 and 20 story models at DBE level.

Through disaggregation, using a software framework OpenSHA (Field et al. 2003), possible values of M, R, and ε are found for the specified hazard levels for the assumed site at Van Nuys, CA. Spectral acceleration, S_a, which corresponds to the DBE seismic hazard level, is 0.85g for the 3 story prototype and 0.23g for the 9 and 20 story prototypes. At the MCE level, S_a is 0.5g for the 3 story and 0.14g for the 9 and 20 story prototypes. For the identified values of spectral acceleration, we obtained multiple combinations of prototype-specific M, R and ε values which, with the site soil conditions, provide necessary input for the attenuation relationship.

Selection of artificially generated ground motions from the full event set was based on their spectral accelerations at the 1st and 2nd mode periods of the prototype SC-MRFs. The 9 and 20 story prototypes have similar periods, therefore the subset of ground motions at the DBE level, shown in Fig. 3, was used in the nonlinear analyses of both buildings. The response design spectrum (IBC(DBE)) is the target spectrum. A tolerance factor was determined to include exactly 1,000 events at the DBE level and another 1,000 at the MCE level within the boundary at T_1 and T_2 of the prototypes. For the 3 story prototype the tolerance factor was found to be 1.329 at the DBE level, and 1.555 at the MCE level; for the 9 and 20 story prototypes, the tolerance factors at the DBE and MCE levels were 1.518 and 1.574, respectively. Therefore, four subsets of synthetic records were selected for the three prototypes.

Nonlinear Structural Model and the Design Procedure Parameters

For the nonlinear time history analyses of the prototype buildings, 2-D models were developed in OpenSees (McKenna and Fenves 2006). The mass of the structure is concentrated at the floor levels of the "leaning column", which is connected to the frame through nonlinear axial springs representing collector beams. The frame model consists of elastic and inelastic elements for beams and columns, and has connection elements modeling the gap behavior, panel zone, ED device, shear support, post-tensioning strands, and the transfer of inertia forces from the floor diaphragms to the SC-MRFs through the collector beams. Fig. 4 shows the model of the beam to column connection.

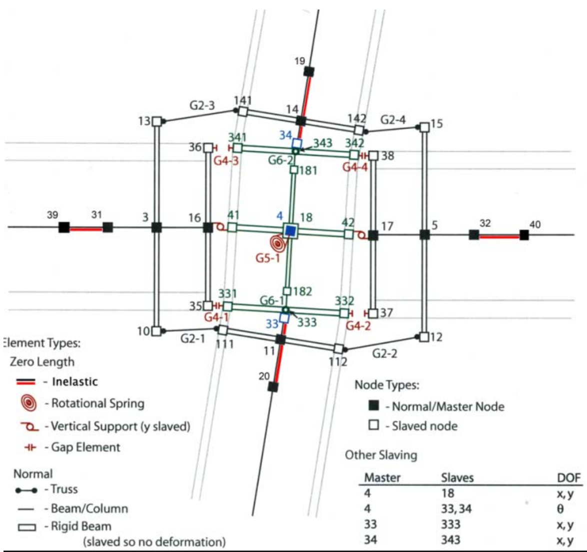

Figure 4. Nonlinear model of the SC-MRF connection.

Seismic demand obtained in the simulations was compared to the predicted demand values given in the design procedure outlined by Garlock (2007). The predicted roof drift demand, $\theta_{roof,\,DBE}$ in Table 1, is based on the equal displacement principle, and it depends on the period correction factor, C_T, damping correction factor C_ξ, and the response modification factor, R, used to define the design base shear, V_{des}. The total height of frame above ground is h_f, and $\Delta_{el\text{-}des}$ is the roof displacement from the linear elastic analysis of the frame corresponding to V_{des}. The story drift demand, θ_{DBE}, is estimated directly from the roof drift, by using a factor C_θ, as seen in Eq. 2. The value for C_θ is based on studies on a 6 story prototype by Rojas (2005), and is used in the design of all three prototypes. Garlock (2002) shows that PT frame beams, columns, and panel zones remain essentially elastic under earthquake loading. Therefore, the elastic story drift, θ_e, is subtracted from the total story drift, θ to estimate the connection relative rotation demand, θ_r, (i.e., $\theta_r = \theta - \theta_e$) as shown in Eq. 3 (Table 1). $K_{f\Delta}$ is the initial (elastic) frame stiffness equal to the base shear divided by the roof displacement and V_{DBE} and V_{MCE} are the base shear demands for the DBE and MCE considering overstrength factors. Eqs. 1, 2 and 3 define the predicted demands, i.e., the "design" values, which are compared to the demands obtained in the nonlinear analyses.

Table 1. Seismic demand predicted by the design procedure.

Roof drift (Eq. 1)	Story drift (Eq. 2)	Relative rotation (Eq. 3)
$\theta_{roof,DBE} = \dfrac{C_{\xi} C_T R \Delta_{el-des}}{h_f}$	$\theta_{DBE} = C_{\theta}\theta_{roof,DBE}$ $where: C_{\theta} = 1.5$	$\theta_{r,DBE} = \theta_{DBE} - \dfrac{C_{\theta} V_{DBE}}{K_{f\Delta} h_f}$

Comparison of SC-MRF Response to the Predicted Demand and Limit State Reliability

Fig. 5 shows the maximum demands obtained in the nonlinear analyses for the roof drift, θ_{roof}, story drift, θ, and beam-column relative rotation, θ_r. The predictions for the 3 story prototype are close to the upper bound of the data obtained in the analyses. The 9 story predictions compare reasonably well to the recorded data, and the 20 story predictions are approximately equal to the average data. These observations are summarized in Table 2, in terms of the percent probability of exceeding the design values.

It was noted earlier that a value of C_{θ}=1.5 was used to design all prototypes. Table 2 shows average C_{θ} values obtained for each prototype. Based on these observations, we recommend C_{θ} to equal 1.1 for buildings with 3 stories or less, 1.6 for 9 stories or more, and to interpolate inbetween. The impact of C_{θ} on the design predictions is shown in Eqs. 2 and 3 from Table 1. There is a linear correlation between C_{θ} and the predicted maximum values for θ and θ_r. The effect of C_{θ} on the relationship between θ and θ_r (as shown in Eq. 3) can be seen in Fig. 6. The design lines representing Eq. 3 are based on C_{θ}=1.5, and are shown next to the data obtained in the nonlinear analyses. In Fig. 6 we see that the design equation best matches the recorded data for the 20 story prototype, whereas the 9 story, and most prominently the 3 story prototype, require an improved prediction. By revising C_{θ} the design lines move towards the data only modestly. Note that changing C_{θ} only affects those designs controlled by the seismic forces, namely the 3 and 9 story prototypes, since the 20 story prototype was largely controlled by a wind load criterion, as mentioned previously. By introducing a multiplier F to Eq. 3 we arrive at Eq. 4, which correlates well with the data for all prototypes of a given number of stories, n, as shown in Fig. 6.

$$\theta_{r,DBE} = \theta_{DBE} - F\frac{C_{\theta} V_{DBE}}{K_{f\Delta} h_f}, \quad where: \; F = \frac{n(n-2)}{10} \le 1.0 \tag{4}$$

Fig. 8a plots a cumulative distribution function (CDF), which is another way of presenting the data in Table 2, and it indicates the probability that θ_r will be at most that indicated on the abscissa. It is seen, for example, that there is an 80% probability of not exceeding the design value of θ_r = 0.021 in the 20 story prototype in a seismic event at the MCE level. For the limit state reliability analysis we use the seismic demand curves (Fig. 8a) and the capacity curves (Fig. 8b) to find the combined probability of the demand exceeding the capacity

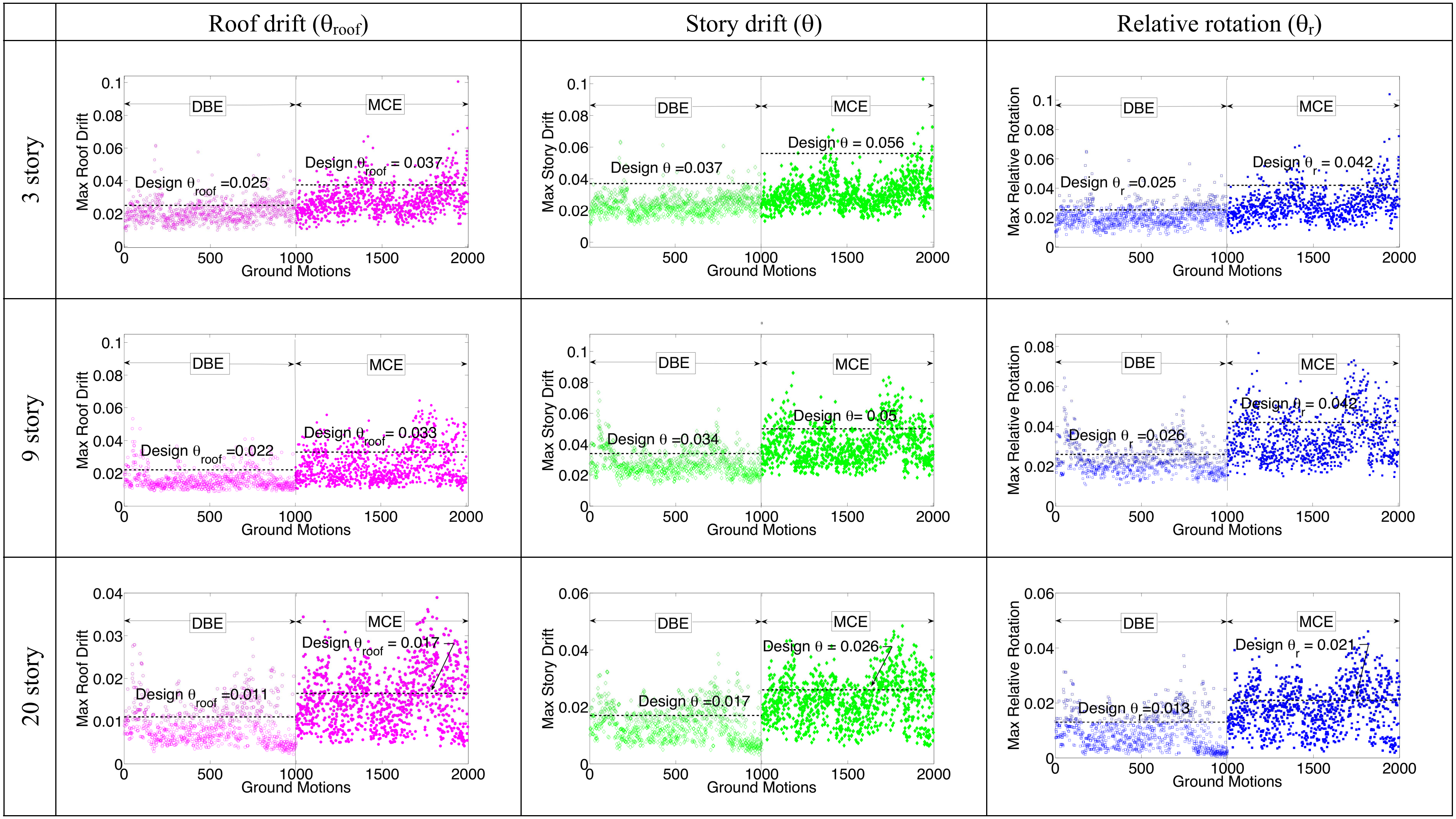

Figure 5: Maximum recorded and predicted seismic demand in every prototype for DBE and MCE ground motions

at each level. The capacity curves are based on Eq. 5, which is a closed form solution that relates relative rotation at the point of strand yielding ($\theta_{r,s}$) to the beam and strand stiffness (k_b and k_s, respectively), number of PT strands (N_s), strand yield force (t_y), initial posttensioning force (t_0), and beam depth ($2d_2$), at each level (Garlock 2007). Based on an assumption that t_y (a material-related uncertainty), and t_0 (a construction-related uncertainty), are random variables, Eq. 5 yields a normally distributed capacity curve (Dobossy et al. 2006). By convolving the demand and capacity distributions for each level,

Table 2. Percent probability of exceeding design values θ_{roof}, θ and θ_r, and C_θ factor

		θ_{roof}	θ	θ_r	C_θ
3 story	DBE	24	2	10	1.1
	MCE	15	1	4	
9 story	DBE	12	20	18	1.6
	MCE	24	20	13	
20 story	DBE	28	29	14	1.6
	MCE	40	33	20	

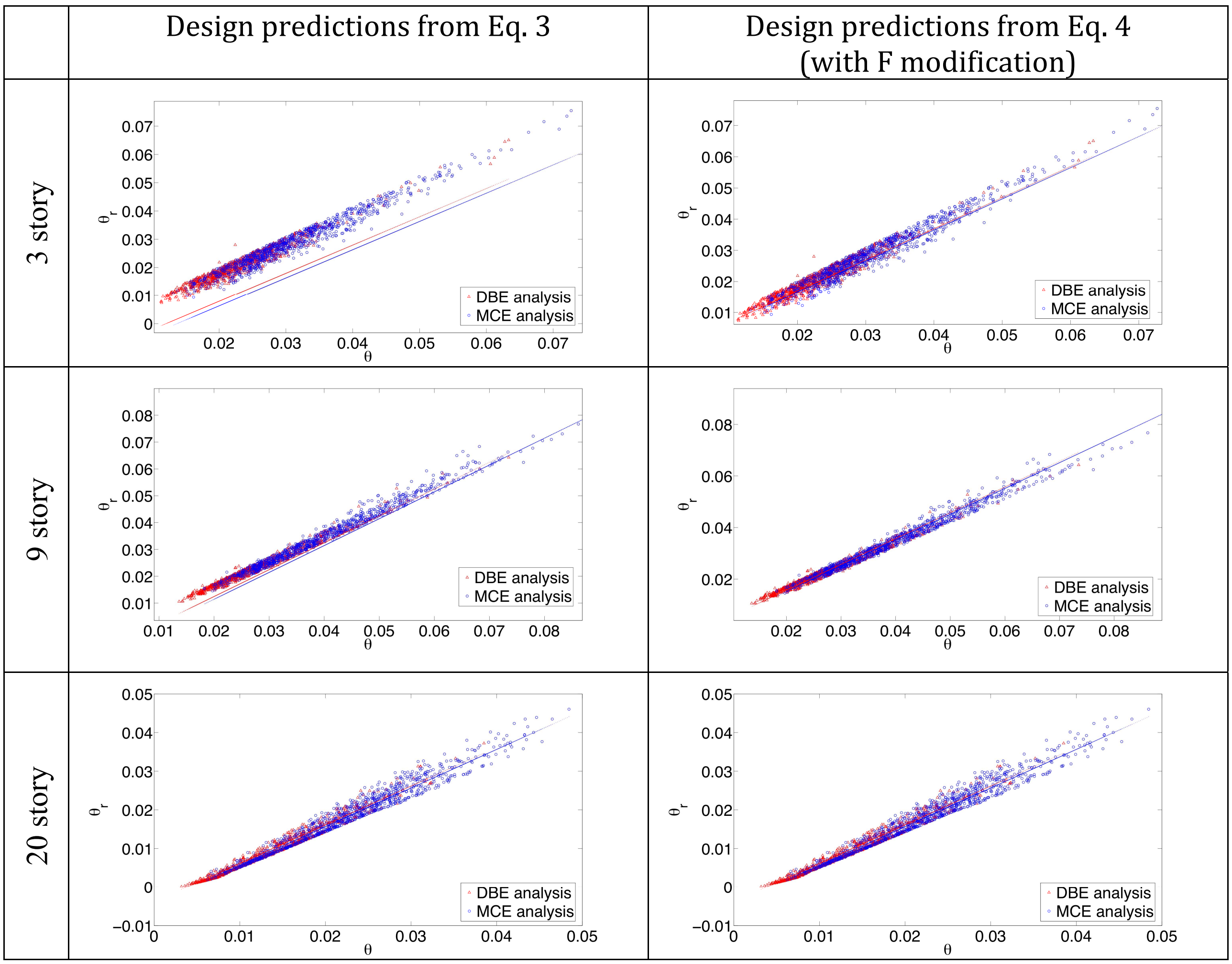

Figure 6. Evaluation of design predictions based on seismic response data

we arrive at the probability of reaching a limit state of strand yielding, as shown in Eq. 6. Using this methodology, we find that the probability of strand yielding in the 3 story prototype is negligible. It varies between 0 and 4% in the 9 story, and between 0 and 7% in the 20 story prototype, with the exception of the 2nd and 3rd levels in the 20 story building, where that probability reaches 12% and 15%, respectively.

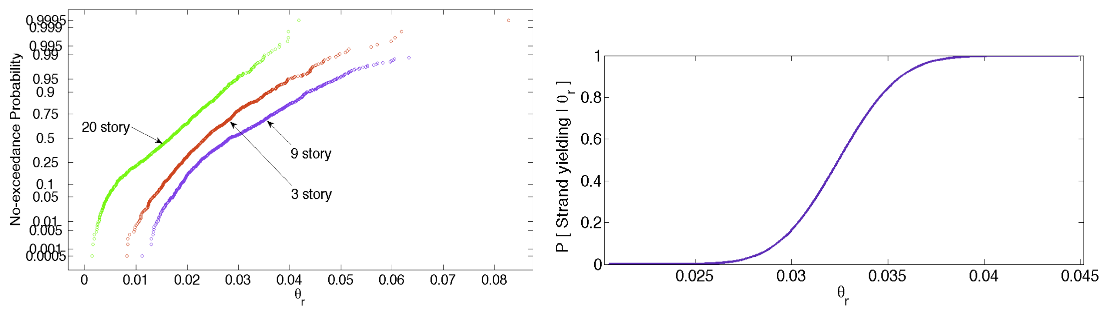

(a) (b)

Figure 8. Limit state probability: (a) Relative rotation demand at MCE level; (b) Capacity CDF of strand yielding in terms of relative rotation at level 6 in the 20 story prototype

$$\theta_{r,s} = \frac{N_s(t_y - t_0)}{2d_2} \cdot \frac{k_b + k_s}{k_b k_s} \tag{5}$$

$$P_{LS} = P[D>C] = \sum_{all\_d} P[D>C \mid D = d] \bullet P[D = d] \tag{6}$$

Summary and Conclusions

This paper presented a continuation of the previous study on developing a reliability-based methodology to evaluate the sensitivity of SC-MRFs to specific design parameters and to validate or improve the design recommendations given previously by Garlock et al. (2007). Three prototype frames (3, 9 and 20 story high) are subject to Monte Carlo simulations of realistic synthetically generated ground motions and peak responses are recorded. The results indicate that the probability of exceeding the design values (such as roof drift, story drift and beam-column relative rotation) varies slightly with prototype height, and is consistent with the results obtained in an earlier study, which used 40 natural, unscaled seismic records. These findings validate the use of realistic, synthetically generated ground motions in probabilistic reliability-based design, in areas where representative natural records are scarce.

The effect of the design parameter C_θ on the estimated demand values was investigated. An improved predictive relationship between the beam-column relative rotation and the story drift is proposed. Future work involves redesigning of the frames with this new prediction and evaluating the response of the new design.

The probability of system failure based on reaching the limit state of strand yielding is calculated. Acceptable level of such probability is based on an engineer's judgment, therefore these results can be used to inform the performance-based design decisions.

In general, prototype responses were found to be adequate, as was the reliability-based methodology for developing the performance-based design procedure. Future work includes plans for a comprehensive limit state reliability analysis, where limit states other than PT strand yielding would be investigated.

Acknowledgements

This material is based upon work supported by American Institute of Steel Construction (AISC) and the National Science Foundation (NSF) under Grant No. 0420974. Any opinions, findings, and conclusions expressed in this material are those of the authors and do not necessarily reflect the views of the sponsors. The authors would also like to thank Jie Li, Mark Dobossy and Raghav Pant for their contributions.

References

Minimum Design Loads for Buildings and Other Structures, 2006. *ASCE Standard*, ASCE/SEI 7-05, Reston, VA

Building Seismic Safety Council, 1997. NEHRP Recommended Provisions for Seismic Regulations for New Buildings and Other Structures. Part 1 – Provisions. *Rep. No. FEMA-302*, for the Federal Emergency Mgmt Agency, Washington, D.C.

Chiou, B., Darragh, R., Gregor, N., and Silva, W., 2008. NGA Project Strong-Motion Database, *Earthquake Spectra*, 24(1), 23-44.

Chou, C. C., Chen, J. H., Chen, Y. C. and Tsai, K. C., 2006. Evaluating performance of post-tensioned steel connections with high-strength strands, *Earthquake Engineering and Structural Dynamics* 35 (9), 1167–1185.

Christopoulos, C., Filiatrault, A., Uang, C.-M., Folz, B., 2002. Posttensioned Energy Dissipating Connections for Moment-Resisting Steel Frames, *Journal of Structural Engineering*, ASCE, 128(9), 1111-1120.

Dobossy, M, Garlock, M., and VanMarke, E., 2006. “Comparison of two self-centering steel moment frame modeling techniques: explicit gap models, and non-linear rotational spring models”, *Proceedings of the 4th International Conference on Earthquake Engineering*, Taipei, Taiwan, October

Field, E. H., Jordan, T. H., and Cornel, C. A., 2003. OpenSHA: A developing community-modeling environment for seismic hazard analysis, *Seismological Research Letters*, 74(4), 406-419.

Garlock, M. M., Ricles, J. M., Sause, R., Peng, S.W., Zhao, C., and Lu, L.-W., 1998. Post-Tensioned Seismic Resistant Connections for Steel Frames, *Structural Stability Research Council Conference Workshop*, Atlanta, Georgia.

Garlock, M, Ricles, J., and Sause, R., 2005. Experimental Studies on Full-Scale Post-Tensioned Steel Connections, *Journal of Structural Engineering*, ASCE, 131(3).

Garlock, M, Sause, R., and Ricles, J., 2007. Behavior and Design of Post-Tensioned Steel Frames, *Journal of Structural Engineering*, ASCE, 133(3), 389-399.

Garlock, M, Li, J. and Vanmarcke, E., 2009. Floor diaphragm design of steel self-centering moment frames, *Proceedings of the Sixth International Conference on Behavior of Steel Structures in Seismic Areas*, *STESSA,* Philadelphia, PA, August.

Herning, G., Garlock, M., and Vanmarcke, E. 2009. Evaluation of design procedure for steel self-centering moment frames, *Proceedings, Steel Strucutres in Seismic Areas (STESSA)*, Philadelphia, PA, August.

International Code Council, 2000. *International Building Code*, Falls Church, Virginia.

McKenna, F., & Fenves, G. L., 2006. Opensees 1.7.0. Computer Software. UC Berkeley, Berkeley, CA.

Pant, R. and Vanmarcke, E., 2009. New attenuation models for earthquake intensity and frequency-content indicators, *in preparation for submission to Earthquake Spectra*

Ricles, J., Sause, R., Garlock, M., and Zhao, C., 2001. Post-Tensioned Seismic Resistant Connections for Steel Frames, *Journal of Structural Eng*, ASCE, 127(2).

Rojas, P., Ricles, J.M., and R. Sause, 2005. Seismic Performance of Post-Tensioned Steel MRFs With Friction Devices, *Journal of Structural Engineering*, ASCE, 131(4), 529-540.

Sabetta, F., Pugliese, A., 1996. Estimation of response spectra and simulation of nonstationary earthquake ground motions, *Bulletin of the Seismological Society of America*, 86(2), 337-352.